Pergamon

Int. J. Heat Mass Transfer. Vol. 41, No. 15, pp. 2335–2346, 1998

Printed in Great Britain
0017–9310/98 $19.00+0.00

PII: S0017–9310(97)00336–0

Reacting stagnation flows in catalytic porous beds

CHIN-TSAU HSU† and HUILI FU

Department of Mechanical Engineering, Hong Kong University of Science and Technology, Clear Water Bay, Kowloon, Hong Kong

(*Received* 1 *April* 1997 *and in final form* 23 *October* 1997)

Abstract—Singular perturbation analysis is employed to investigate the heat and mass transfer of chemically-reactive steady stagnation flows in catalytic porous beds, under the assumption of a thin thermal boundary layer. Results indicate that the control parameters for the reactant concentration are those associated with Arrhenius kinetics, i.e., the reaction rate constant, the activation energy and the fluid temperature feeding the bed. On the other hand, the governing parameters for the temperature profiles are those associated with the chemical reaction heat and the thermal conductivity. The role of the mass diffusivity is not important to reactant concentration and temperature, once the mass diffusion boundary layer remains within the thermal boundary layer. Brinkman's viscous layer near the impermeable wall is included in the present analysis; however, its effect on the heat transfer and chemical reaction characteristics is found to be negligible. © 1998 Elsevier Science Ltd. All rights reserved.

1. INTRODUCTION

Great attention has been given to chemically reacting flows in porous media because of their practical applications in the petrochemical and petroleum refining industries, as well as in the environmentally clean utilization of energy. For example an ammonia production line in the petrochemical industry consists of about seven fixed bed catalytic reactors for the processes of steam reforming of methane, water–gas shift reaction, ammonia synthesis, etc. [1]. In the clean utilization of energy, examples include industrial ceramic porous burners [2], catalytic converters in an exhaust-gas system [3], and others. A catalytic converter is essentially a porous bed where residual hydrocarbons and carbon monoxide exhausted from an internal combustion engine are converted into carbon dioxide and water vapor at a relatively low temperature. In the above mentioned catalytic reactors/convertors, the chemical processes range from strong endothermic (steam reforming of methane) to strong exothermic (exhaust gas conversion).

The physical geometry shows that the flows in the catalytic reactor are usually the combination of a one-dimensional flow and a stagnation point flow. Attention has been given to the one-dimensional flow because it is more commonly encountered in the reactors. Therefore, in this study we focus on the stagnation point flow in a packed catalytic bed impinging on an impermeable wall.

There exist several works on the reacting stagnation flows in pure gas phase, particularly in relation to the flame combustion. Chao and Law [4] studied the propagation of a premixed stagnation point flame based on constant density approximation, while Sato and Tsuji [5] on variable approximation. Law and Sivashinsky [6], and Giovangigli and Candel [7] studied the stagnation point flame impinging on a catalytic surface. In these analyses, a one-step irreversible reaction based on Arrhenius kinetics with high activation energy was used.

Although great effort has been devoted to heat transfer in porous media, little attention has been given to chemically reacting flows until recently. Vijoen and Hlavacek [8] investigated the chemically driven convection in a porous medium at low temperature. Chen *et al.* [9] studied the premixed flame in a porous medium and found that thermal radiation promotes flame stability and propagation speed. More recently Chao *et al.* [10] analyzed the non-premixed burning of a condensed fuel in porous media with a naturally convective oxidizer adjacent to the impermeable wall.

Exothermic reactive flows impinging on a layer of catalytic porous bed adjacent to an impermeable wall were investigated by Chao *et al.* [11]. They assumed that the thermal conductivity ratio of the bed to the fluid is very large to justify as a perturbation parameter and neglected the viscous effect of fluid near the impermeable wall. By considering the special situation where the activation energy of the catalytic reaction is very low and proportional to the root square of the bed/fluid thermal conductivity ratio, they analyzed two cases when the thickness of the thermal diffusion layer is much thicker or thinner than the thickness of the porous bed. Their results showed that the most

† Author to whom correspondence should be addressed. Tel: 852 2358 7188. Fax: 852 2358 1543. E-mail: mecthsu@ust.hk.

NOMENCLATURE

B	velocity strain rate
c	chemical reaction rate constant
c_p	specific heat of fluid
c_{ps}	specific heat of solid particles of the bed
D_e	effective mass diffusivity
G	normalized concentration for outer solution
g	normalized concentration for inner solution
H	thickness of the catalytic bed
k_e	effective conductivity of the catalytic bed
K	permeability of the catalytic bed
Le	Lewis number
Pe	Peclet number
P_n	ratio of Brinkman's layer thickness to H
R	gas constant
Q	chemical reaction heat per unit mass rate
T	temperature
T_a^*	normalized activation energy
T_∞^*	normalized absolute temperature of incoming fluid
u	velocity component along the catalytic bed
v	velocity component normal to the catalytic bed
$\dot{W}$	normalized reaction rate
Y	concentration.

Greek symbols

α_e	effective thermal diffusivity
γ_m	dimensionless parameter of reaction rate constant
γ_T	dimensionless parameter of chemical reaction heat
ΔT	temperature difference, $\lvert T_w - T_\infty \rvert$
ε	reaction of the thermal boundary layer thickness to H
θ	normalized temperature for inner solution
Θ	normalized temperature for outer solution
μ	viscosity of fluid
ρ	density of fluid
ϕ	porosity of the catalytic bed.

Subscript

0	$O(1)$ solution
1	$O(\varepsilon)$ solution
λ	$O(\varepsilon^\lambda)$ solution
w	values at the impermeable wall
∞	values at far away from the catalytic bed.

Superscripts

^	inner variable.

salient physical features occur only when the catalytic porous bed is much thicker than the thermal boundary layer.

Although this study was initially motivated by the work of Chao *et al.* [11], here we have investigated more generally the reacting stagnation point flows in catalytic beds where the chemical reaction can be endothermic or exothermic. In addition, we have also included the viscous effect and relaxed the assumption of very low activation energy. Attention was given only to the case when the catalytic porous bed is much thicker than the thermal boundary layer near the impermeable wall. Naturally the thickness ratio of the thermal boundary layer to the catalytic bed becomes the small parameter which warrants a singular perturbation analysis. The inclusion of the viscous effect leads to the existence of the Brinkman's viscous layer near the impermeable wall. The effect of the Brinkman's layer on the reacting flow is then characterized by the thickness ratio of the Brinkman's layer to the thermal boundary layer. Solutions have been obtained for different values of Lewis number which measures the ratio of mass and thermal diffusion rates of reactant, as well as for different values of reaction rate parameters. The effects of these parameters on flow field, heat transfer and reaction characteristics are discussed.

2. FORMULATION

2.1. *Problem definition*

For stagnation flows impinging on a catalytic porous bed adjacent to an impermeable wall, the results of Chao *et al.* [11] showed that the configuration above the catalytic porous bed has little consequence to the performance of the catalytic bed provided the bed is much thicker than the thermal boundary layer. For simplicity, we idealize our problem by considering a semi-infinite extent porous medium with a two-dimensional steady stagnation flow toward an impermeable wall at $y = 0$ as shown in Fig. 1. Near the impermeable wall is a packed catalytic bed of thickness H. Above the catalytic bed lays the inert bed from $y = H$ to ∞. We also assume that the catalytic and the inert beds have the same packing structure which yields the same permeability, K, and hence

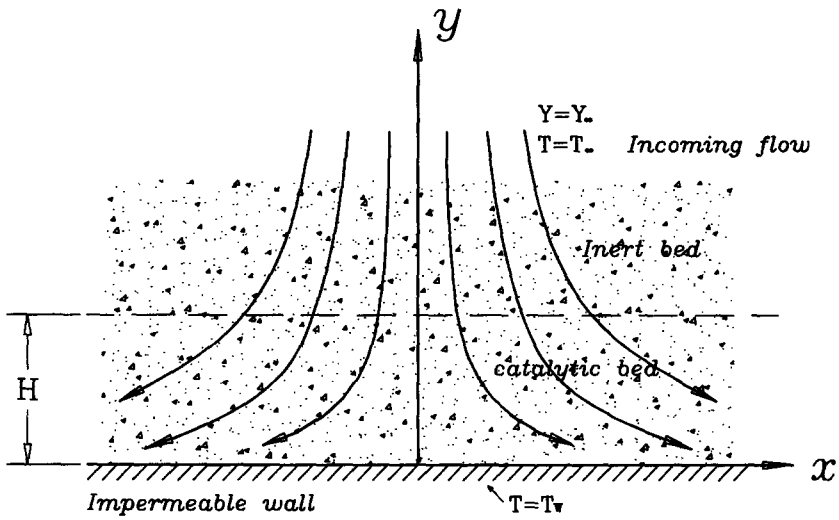

Fig. 1. The schematic of the problem and the coordinate system.

the streamlines do not experience the interface between the inert and catalytic beds. As shown in Fig. 1, the flow at infinity has a temperature T_∞ and carries a reactant of concentration Y_∞. As the flow enters the catalytic bed, chemical reactions take place to cause the changes in temperature and the concentration. Here, we have studied the case of a constant temperature T_w at the impermeable wall. (The case of constant heat flux can be easily adopted in the present analysis.) The conduction results in a thermal boundary layer near the impermeable wall. Because the impermeable wall represents a boundary barrier across which no mass transfer can occur, a mass diffusion layer is formed near the impermeable wall. The viscous effect of the impermeable wall also leads to the Brinkman's viscous layer at the proximity of the wall. In this study, it is assumed that the thickness of the catalytic bed is very large compared with the thickness of the viscous layer, the thermal boundary layer and of the mass diffusion layer.

2.2. *Governing equations*

It is further assumed that the porosity of the medium, ϕ, is constant, the fluid density ρ is constant, the Reynolds number based on particle diameter is low so that Darcy's law is applicable, the heat transfer process in the medium is in local thermal equilibrium, the viscous dissipation is negligible, the buoyant effect is neglected, and that the chemical reaction is simplified by a one-step reaction according to Arrhenius kinetics. It is also further assumed that the temperature change in the catalytic bed is small compared to the temperature of incoming fluid so that the fluid properties can be regarded as constants. Under these assumptions and after normalized with the length scale H and the velocity scale BH were B is the velocity strain rate, the conservation equations for the fluid mass and momentum are

$$\frac{\partial u}{\partial x}+\frac{\partial v}{\partial y}=0 \tag{1}$$

and

$$u=-\frac{\partial p}{\partial x}+P_n^2\left(\frac{\partial^2 u}{\partial x^2}+\frac{\partial^2 u}{\partial y^2}\right)$$

$$v=-\frac{\partial p}{\partial y}+P_n^2\left(\frac{\partial v^2}{\partial x^2}+\frac{\partial^2 v}{\partial y^2}\right) \tag{2a,b}$$

subjected to the boundary conditions,

$$u=v=0 \quad \text{at } y=0$$

$$u=x, v=-y \quad \text{as } y\to\infty. \tag{3a,b}$$

In equation (2), $P_n=\sqrt{K/(\phi H^2)}$ represents the ratio of Brinkman's viscous layer thickness to H and is usually very small.

Similarly, if the temperature T and the mass concentration Y of the reactant are normalized into $\Theta=(T-T_\infty)/\Delta T$ and $G=Y/Y_\infty$, where $\Delta T=|T_w-T_\infty|$, with the subscripts w and ∞ denoting the values at the impermeable wall and at infinity, respectively, the non-dimensional conservation equations for energy and mass-diffusion, respectively, are

$$u\frac{\partial\Theta}{\partial x}+v\frac{\partial\Theta}{\partial y}=\frac{1}{Pe}\left[\frac{\partial}{\partial x}\left(\frac{\partial\Theta}{\partial x}\right)+\frac{\partial}{\partial y}\left(\frac{\partial\Theta}{\partial y}\right)\right]-\gamma_T\dot{W} \tag{4}$$

and

$$u\frac{\partial G}{\partial x}+v\frac{\partial G}{\partial y}=\frac{1}{Pe\,Le}\left[\frac{\partial}{\partial x}\left(\frac{\partial G}{\partial x}\right)+\frac{\partial}{\partial y}\left(\frac{\partial G}{\partial y}\right)\right]+\gamma_m\dot{W} \tag{5}$$

where the dimensionless chemical reaction rate $\dot{W}$,

normalized by cY_∞ with c being the reaction rate constant, is described by

$$\dot{W} = \begin{cases} 0 & y > 1 \\ G\exp\left\{-\dfrac{T_a^*}{\Theta + T_\infty^*}\right\} & 0 < y < 1 \end{cases} \quad (6)$$

The proper boundary conditions for equations (4), (5) are

$$\Theta = 1, \quad \frac{\partial G}{\partial y} = 0 \quad \text{at } y = 0$$

$$\Theta = 0, \quad G = 1, \quad \text{as } y \to \infty. \quad (7a,b)$$

In equations (4)–(6), $Pe = BH^2/\alpha_e$ is the Peclet number, $Le = \alpha_e/D_e$ the Lewis number, $\gamma_m = c/\rho B$ the non-dimensional chemical reaction rate constant (also interpreted as Damkohler number), $\gamma_T = QcY_\infty/[(\rho c_p)_m B\Delta T]$ the non-dimensional chemical reaction heat, T_a^* the non-dimensional activation energy normalized by $R\Delta T$ with R being the gas constant and $T_\infty^* = T_\infty/\Delta T$ the non-dimensional absolute temperature of the incoming flow. In the above definitions, Q is the heat generation per unit mass rate of reaction and $(\rho c_p)_m = \phi\rho c_p + (1-\phi)\rho_s c_{ps}$ the volume-averaged heat capacity. The effective thermal diffusivity, α_e, is usually contributed from a stagnant diffusivity and a thermal dispersion. It is known that the thermal dispersion depends on the Reynolds number based on the length scale of the pore structure in the medium. For simplicity, however, we assume that α_e is constant. This assumption is plausible at low Reynolds number, and is consistent with the Darcy's law assumption in the momentum equation. Similarly, we also assume that the effective mass diffusion, D_e, is constant.

3. VELOCITY FIELDS

Since equations (1) and (2) with the boundary conditions (3) are de-coupled from the energy and mass-diffusion equations, they can be solved independently. The solutions to equations (1) and (2) satisfying (3) are obtained by eliminating pressure terms first and then following the procedures given on page 96 of Schlichting [12]; the results are

$$u = x[1 - \exp(-y/P_n)]$$

$$v = -y + P_n[1 - \exp(-y/P_n)]. \quad (8a,b)$$

Note that equation (8b) shows that v is a function of y only. Because P_n is very small, the exponential terms in equation (8) can be usually omitted, except at the proximity of the impermeable wall. Therefore, in view of a far field the velocity field behaves like $u = x$ and $v = -y + P_n$, i.e., the impermeable wall appears as if it were located at $y = P_n$. The Brinkman's viscous effect procedures a displacement thickness of order of P_n. Figure 2 shows the profiles of u/x and $-v$ for $P_n = 0.01$, 0.03 and 0.10. Clearly, the Brinkman's layer thickness is of order P_n.

4. TEMPERATURE AND CONCENTRATION PROFILES

We now solve equations (4)–(6) satisfying the boundary condition (7). From equations (4) and (5) we notice that $Pe^{-1/2}$ represents the thickness ratio of thermal boundary layer to the catalytic bed and that $Le^{1/2}$ represents the thickness ratio of thermal boundary layer to the mass diffusion layer. In this study, we assume that $Pe \gg 1$, i.e., the catalytic bed is much thicker than the thermal boundary layer near the impermeable wall. The parameters Le, γ_T and γ_m are regarded as of order $O(1)$. Hence, the mass diffusion layer is also much thinner than the catalytic bed, but comparable to the thermal boundary layer. In practical operation of catalytic beds, the value of γ_m is negative and γ_T can be positive or negative for endothermic or exothermic reactions, respectively. The parameters T_∞^* and T_a^* are usually large; however, their ratio is assumed to be of manageable order for numerical computation. This is different from the treatment of Chao *et al.* [11] where T_a^*/T_∞^* was assumed to be small.

Singular perturbation analyses

Exact solutions to the equation system (4)–(7) cannot be obtained without invoking directly a numerical procedure. To gain more insights into the physics of the problem, we analyze the equation system with a singular perturbation method, using $\varepsilon = Pe^{-1/2}$ as a small parameter. Due to the mathematic complexity of the exponential term appearing in equation (6), the perturbation analysis will be carried out only up to $O(\varepsilon)$.

Outer expansions

In the outer region where y is of $O(1)$, the outer variables are expanded into

$$\Theta = \Theta_0 + \varepsilon\Theta_1 + \cdots$$

$$G = G_0 + \varepsilon G_1 + \cdots$$

$$\dot{W} = \dot{W}_0\varepsilon + \dot{W}_1 + \cdots. \quad (9)$$

The substitution of equation (9) into equations (4)–(7) and expanding for small ε leads to $O(1)$:

$$u\frac{\partial\Theta_0}{\partial x} + v\frac{\partial\Theta_0}{\partial y} = -\gamma_T\dot{W}_0$$

$$u\frac{\partial G_0}{\partial x} + v\frac{\partial G_0}{\partial y} = \gamma_m\dot{W}_0 \quad (10a,b)$$

$$\dot{W}_0 = \begin{cases} 0 & y > 1 \\ G_0\exp\left\{-\dfrac{T_a^*}{\Theta_0 + T_\infty^*}\right\} & 1 \geqslant y \geqslant 0 \end{cases} \quad (10c)$$

subject to boundary conditions,

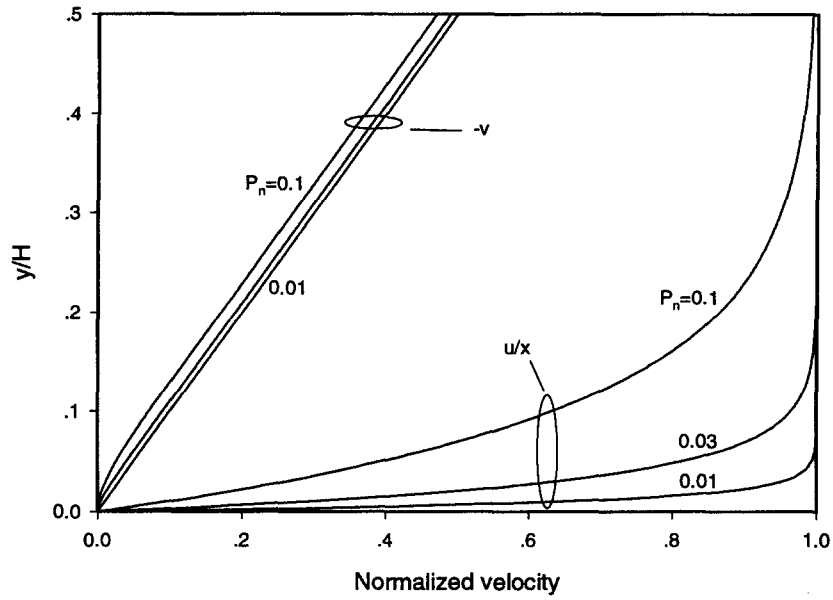

Fig. 2. The velocity profiles of stagnation flows in porous beds.

$$\Theta_0 = 0, \quad G_0 = 1 \quad \text{as } y \to \infty \tag{11}$$

and $O(\varepsilon)$:

$$u\frac{\partial \Theta_1}{\partial x} + v\frac{\partial \Theta_1}{\partial y} = -\gamma_T \dot{W}_1$$

$$u\frac{\partial G_1}{\partial x} + v\frac{\partial G_1}{\partial y} = \gamma_m \dot{W}_1 \tag{12a,b}$$

$$\dot{W}_1 = \begin{cases} 0 & y > 1 \\ \left[G_1 + \Theta_1 \dfrac{T_a^*}{(\Theta_0 + T_\infty^*)^2} G_0\right] \exp\left\{-\dfrac{T_a^*}{\Theta_0 + T_\infty^*}\right\} & 1 \geqslant y \geqslant 0 \end{cases} \tag{12c}$$

subject to the boundary conditions,

$$\Theta_1 = G_1 = 0 \quad \text{as } y \to \infty. \tag{13}$$

Note that the conditions at $y = 0$ for Θ_0 and G_0, as well as for Θ_1 and G_1, cannot be prescribed since the higher derivatives in the governing equations are omitted. From the above outer expansion, it appears that the diffusion terms in equations (4) and (5) do not play a role up to $O(\varepsilon)$, i.e., the outer solution up to this order behaves as if the medium is neither conductive nor diffusive. The transport is dominated by the convection and reaction.

Outer solutions of O(1)

We now solve the equation system (10) and (11) of $O(1)$. The elimination of the right-hand side of (10a,b) gives

$$u\frac{\partial Z_0}{\partial x} + v\frac{\partial Z_0}{\partial y} = 0 \tag{14}$$

where

$$Z_0 = \gamma_m \Theta_0 + \gamma_T G_0. \tag{15}$$

In this study, the Brinkman's viscous sub-layer is imbedded in the thermal boundary layer; therefore, we have $u = x$ and $v = -y$ in the outer region. By invoking $u = x$ and $v = -y$ and introducing the orthogonal streamline coordinate system (n, s) for the stagnation flow, i.e., $xy = n$ and $(x^2 - y^2)/2 = s$ (where n and s are normal to and along the streamlines, respectively), equation (14) reduces to $\partial Z_0/\partial s = 0$, i.e., Z_0 remains constant along a streamline. The boundary conditions (11) then suggest that $Z_0 = \gamma_T$ in the entire outer region. In fact, Z_0 is the total active potential available for reaction of the incoming flow.

In the inert bed where $\dot{W}_0 \equiv 0$, we have

$$u\frac{\partial \Theta_0}{\partial x} + v\frac{\partial \Theta_0}{\partial y} = 0$$

$$u\frac{\partial G_0}{\partial x} + v\frac{\partial G_0}{\partial y} = 0. \tag{16a,b}$$

Hence, Θ_0 and G_0 also remain constant along streamlines. The boundary conditions (11) at $y \to \infty$ lead to $\Theta_0 = 0$ and $G_0 = 1$ for $1 \leqslant y < \infty$, independent of x. Thus, the boundary conditions at the interface of inert and catalytic beds are given by

$$\Theta_0 = 0, \quad G_0 = 1 \quad \text{and} \quad Z_0 = \gamma_T \quad \text{at } y = 1. \tag{17}$$

In the catalytic bed, Z_0 remains constant along streamlines, i.e., $Z_0 = \gamma_T$; however, Θ_0 and G_0 con-

tinuously change due to the chemical reaction. Because $Z_0 \gamma_T$ for all $x =$ and y, equation (15) reads

$$\Theta_0 = \frac{\gamma_T}{\gamma_m}(1 - G_0) \tag{18}$$

in the outer region. By invoking equations (10c) and (18) and $u = x$ and $v = -y$ into equation (10b), the resultant equation, after transforming the coordinate from (x, y) to (n, s) and changing the variable with $\xi = \frac{1}{2}\ln(\sqrt{n^2 + s^2} - s) = \ln y$, becomes

$$\frac{\partial G_0}{\partial(\ln y)} = -\gamma_m G_0 \exp\left\{-\frac{C_a^*}{1 + C_\infty^* - G_0}\right\} \tag{19}$$

where

$$C_a^* = \frac{\gamma_m}{\gamma_T} T_a^*, \quad C_\infty^* = \frac{\gamma_m}{\gamma_T} T_\infty^*.$$

Because the boundary conditions at $y = 1$ are independent of x, the partial derivative becomes the total derivatives; therefore, G_0 is a function of y only. The integration of equation (19) with $G_0 = 1$ at $y = 1$ gives

$$\int_{G_0}^{1} \frac{1}{G_0 F(G_0)} \mathrm{d}G_0 = \gamma_m \ln y \tag{20}$$

where

$$F(G_0) = \exp\left\{-\frac{C_a^*}{1 + C_\infty^* - G_0}\right\}. \tag{21}$$

Equations (20) and (21) suggest that as $y \to 0$, F has to approach a positive constant value, say F^*, and G_0 asymptotically becomes

$$G_0 = C_0 y^\lambda \quad \text{as } y \to 0 \tag{22}$$

where $\lambda = -\gamma_m F^*$. Since $\lambda_m < 0$ (because the reaction always leads to the depletion of reactant) and $F^* > 0$ from equation (21), λ is greater than zero. Hence, $G_0 \to 0$ as $y \to 0$, and $F^* = F(0)$ from equation (21).

By performing the asymptotic expansion to equation (20) for $y \to 0$ and comparing the expansion results with equation (22), the value of C_0 is obtained as

$$C_0 = \exp\left\{\int_0^1 \frac{1}{x}\left\{\exp\left[\frac{C_a^*}{1 + C_\infty^*}\frac{x}{1 + C_\infty^* - x}\right] - 1\right\}\mathrm{d}x\right\}. \tag{23}$$

We also have, as $y \to 0$,

$$G_0 = C_0 y^\lambda \left[1 - \frac{C_a^*}{(1 - C_\infty^*)^2} C_0 y^\lambda + O(y^\lambda)^2\right] \tag{24}$$

and

$$\Theta_0 = \frac{\gamma_T}{\gamma_m}\left[1 - C_0 y^\lambda + \frac{C_a^*}{(1 + C_\infty^*)^2}(C_0 y^\lambda)^2 + O(y^\lambda)^3\right] \tag{25}$$

from equation (18), which are the matching conditions for inner solutions to be obtained later.

Outer solution of $O(\varepsilon)$

Following the procedures for the $O(1)$ solution given above, it can be shown that $Z_1 = \gamma_m \Theta_1 + \gamma_T G_1$ remains constant along streamlines in both inert and catalytic beds. The implementation of the boundary conditions (13) leads to $Z_1 \equiv 0$; hence,

$$\Theta_1 = -\frac{\gamma_T}{\gamma_m} G_1. \tag{26}$$

Similar to the $O(1)$ results, we have $\Theta_1 \equiv G_1 \equiv 0$ in the inert bed. Therefore, the upper boundary conditions for the catalytic bed are

$$Z_1 = \Theta_1 = G_1 = 0 \quad \text{at } y = 1. \tag{27}$$

In the catalytic bed, after invoking equation (26) and following the same analysis procedure for $O(1)$, equation (12) reduces to

$$\frac{\mathrm{d}G_1}{\mathrm{d}(\ln y)} = -\gamma_m G_1 \left[1 - \frac{\gamma_T}{\gamma_m}\frac{T_a^*}{(\Theta_0 + T_\infty^*)^2} G_0\right] \times \exp\left\{-\frac{T_a^*}{\Theta_0 + T_\infty^*}\right\}. \tag{28}$$

Ideally equation (28) can be integrated from $y = 1$–0 using the boundary condition (27); however, the linear property of equation (28) suggests that the magnitude of the solution depends on a multiplication constant which can only be obtained by matching to the inner solution. The matching conditions as inferred from the inner solutions to be obtained later are $\Theta_1 = G_1 = 0$ as $y \to 0$. With the upper boundary condition (27), the only possible solution is $G_1 \equiv 0$, and hence $\Theta_1 \equiv 0$ from equation (26).

Inner expansions

Consider now the region at close proximity of the impermeable heated wall. We first stretch the outer coordinate into the inner coordinate by

$$y = \varepsilon \hat{y} \quad \text{and} \quad x = \hat{x}. \tag{29}$$

The velocity fields in terms of inner variables are

$$u = \hat{u} = \hat{x}[1 - \exp(-\hat{y}/\hat{P}_n)]$$

$$v = \varepsilon \hat{v} = -\varepsilon[\hat{y} - \hat{P}_n[1 - \exp(-\hat{y}/\hat{P}_n)] \tag{30a,b}$$

where $\hat{P}_n = P_n/\varepsilon$ represents the thickness ratio of Brinkman's viscous layer to thermal boundary layer.

Denoting the inner variables by θ and g for the temperatures and concentration, respectively, the governing equations (4)–(6) in terms of the inner coordinate become

$$\hat{u}\frac{\partial \theta}{\partial \hat{x}} + \hat{v}\frac{\partial \theta}{\partial \hat{y}} = \varepsilon^2 \frac{\partial}{\partial \hat{x}}\left(\frac{\partial \theta}{\partial \hat{x}}\right)$$

$$+\frac{\partial}{\partial\hat{y}}\left(\frac{\partial\theta}{\partial\hat{y}}\right)-\gamma_T g\exp\left\{-\frac{T_a^*}{\theta+T_\infty^*}\right\}$$

$$\hat{u}\frac{\partial g}{\partial\hat{x}}+\hat{v}\frac{\partial g}{\partial\hat{y}}=\frac{\varepsilon^2}{Le}\frac{\partial}{\partial\hat{x}}\left(\frac{\partial g}{\partial\hat{x}}\right)$$

$$+\frac{1}{Le}\frac{\partial}{\partial\hat{y}}\left(\frac{\partial g}{\partial\hat{y}}\right)+\gamma_m g\exp\left\{-\frac{T_a^*}{\theta+T_\infty^*}\right\}. \quad (31a,b)$$

The inner limits of the $O(1)$ outer solutions suggests that the inner variables should be expanded into

$$\theta=\theta_0+\varepsilon^\lambda\theta_\lambda+\varepsilon\theta_1+\cdots$$

$$g=g_0+\varepsilon^\lambda g_\lambda+\varepsilon g_1+\cdots. \quad (32a,b)$$

In view that the Brinkman's viscous layer thickness depends on $\hat{P}_n$ only but not on $(\hat{x},\hat{y})$ and that the outer solutions are functions of $\hat{y}$ only, the inner solutions to the order of accuracy under consideration have to be also functions of $\hat{y}$ only, i.e., θ_0, θ_λ, θ_1, g_0, g_λ and g_1 are independent of $\hat{x}$. The dependence of the solutions of $\hat{x}$ may occur only at higher order when the x-derivative diffusion terms in equation 32 into equation (31) become countable. The substitution of equation (31) leads to the following results.

Inner solution of O(1)

The governing equations of θ_0 and g_0 are

$$\hat{v}\frac{\partial\theta_0}{\partial\hat{y}}=\frac{\partial}{\partial\hat{y}}\left(\frac{\partial\theta_0}{\partial\hat{y}}\right)-\gamma_T g_0\exp\left\{-\frac{T_a^*}{\theta_0+T_\infty^*}\right\}$$

$$\hat{v}\frac{\partial g_0}{\partial\hat{y}}=\frac{1}{Le}\frac{\partial}{\partial\hat{y}}\left(\frac{\partial g_0}{\partial\hat{y}}\right)+\gamma_m g_0\exp\left\{-\frac{T_a^*}{\theta_0+T_\infty^*}\right\} \quad (33a,b)$$

subject to boundary conditions,

$$\theta_0=1,\quad \frac{\partial g_0}{\partial\hat{y}}=0,\quad \text{at } \hat{y}=0 \quad (34a,b)$$

and the matching conditions,

$$\theta_0=\frac{\gamma_T}{\gamma_m},\quad g_0=0\quad \text{as } \hat{y}\to\infty. \quad (35a,b)$$

The above boundary conditions for g_0 suggest that the only possible solution for equation (33b) is $g_0\equiv 0$. Therefore, equation (33a) reduces to

$$\hat{v}\frac{\partial\theta_0}{\partial\hat{y}}=\frac{\partial}{\partial\hat{y}}\left(\frac{\partial\theta_0}{\partial\hat{y}}\right) \quad (36)$$

which is characterized by pure conduction/convection. The solution of θ_0 obtained by integrating equation (36) to satisfy the boundary condition (34a) and the matching condition (35a) is

$$\theta_0(\hat{y})=\frac{\left(\gamma_T\Big/\gamma_m-1\right)\int_0^{\hat{y}}E(\eta)\,d\eta}{\int_0^\infty E(\eta)\,d\eta}+1 \quad (37)$$

where

$$E(\eta)=\exp\left[\int_0^\eta\hat{v}\,d\hat{y}\right]$$

$$=\exp\left[-\frac{\eta^2}{2}+\hat{P}_n(e^{-\eta/\hat{P}_n}-1)+\hat{P}_n\eta\right]. \quad (38)$$

Note that from equation (38) θ_0 approaches γ_T/γ_m exponentially as $\hat{y}\to\infty$. Hence, the matching conditions for the $O(\varepsilon)$ outer solutions are $\Theta_1=G_1=0$ as $y\to 0$.

Inner solution of O(ε^λ)

The governing equations for θ_λ and g_λ, after invoking $g_0=0$, are

$$\hat{v}\frac{\partial\theta_\lambda}{\partial\hat{y}}=\frac{\partial}{\partial\hat{y}}\left(\frac{\partial\theta_\lambda}{\partial\hat{y}}\right)-\gamma_T g_\lambda\exp\left\{-\frac{T_a^*}{\theta_0+T_\infty^*}\right\}$$

$$\hat{v}\frac{\partial g_\lambda}{\partial\hat{y}}=\frac{1}{Le}\frac{\partial}{\partial\hat{y}}\left(\frac{\partial g_\lambda}{\partial\hat{y}}\right)+\gamma_m g_\lambda\exp\left\{-\frac{T_a^*}{\theta_0+T_\infty^*}\right\} \quad (39a,b)$$

subject to the boundary conditions,

$$\theta_\lambda=0,\quad \frac{\partial g_\lambda}{\partial\hat{y}}=0\quad \text{at } \hat{y}=0 \quad (40a,b)$$

and the matching conditions,

$$\theta_\lambda=-\frac{\gamma_T}{\gamma_m}C_0\hat{y}^\lambda,\quad g_\lambda=C_0\hat{y}^\lambda\quad \text{as } \hat{y}\to\infty. \quad (41a,b)$$

Equations (39)–(41) can only be solved numerically. This can be done by the simple Runge–Kutta procedure since equations (39) are ordinary differentially equations of y only. Because equation (39b) is linear, the solution for g_λ can be obtained by integrating equation (39b) with the boundary condition (40b) and the condition, $g_\lambda=1$ at $\hat{y}=0$, and then re-normalizing the integrated results to satisfy the matching condition (41b). The solution for θ_λ is then obtained by the integration of equation (39a) using a shooting method to satisfy the conditions (40a) and (41a).

Inner solution of O(ε)

The perturbation equations for θ_1 and g_1 are identical to equation (39) for θ_λ and g_λ, except θ_λ and g_λ being replaced, respectively, by θ_1 and g_1. However, the boundary conditions at the impermeable wall are replaced by

$$\theta_1=0,\quad \frac{\partial g_1}{\partial\hat{y}}=0,\quad \text{at } \hat{y}=0 \quad (42a,b)$$

and the upper matching conditions by

$$\theta_1\to 0,\quad g_1\to 0\quad \text{as } \hat{y}\to\infty. \quad (43a,b)$$

Except for the eigensolutions which may occur at certain critical values of Le, the only possible solutions to satisfy the zero boundary conditions are that

$$g_1(\hat{y}) \equiv \theta_1(\hat{y}) \equiv 0. \quad (44)$$

Composite solutions

The composite solutions are constructed based on the additive principle as described in Van Dyke [13]. Since both the inner and outer solutions of $O(\varepsilon)$ are zero, the composite solutions become

$$\Theta = \Theta_0 + \theta_0 + \theta_\lambda - \Theta_{0m} + O(\varepsilon^2) + O(\varepsilon^{2\lambda})$$

$$G = G_0 + g_0 + g_\lambda - G_{0m} + O(\varepsilon^2) + O(\varepsilon^{2\lambda}). \quad (45a,b)$$

In equation (45a,b), the $O(1)$ outer solutions, Θ_0 and G_0, are computed from equations (18), (20) and (21), the matching expansions, Θ_{0m} and G_{0m}, are obtained from equations (24) and (25), the $O(1)$ inner solution θ_0 is calculated from equations (37) and (38) and $g_0 \equiv 0$, and the $O(\varepsilon^\lambda)$ inner solutions, Θ_λ and g_λ, are obtained by the direct integration of equations (39)–(41).

The singular perturbation analysis given above leads to two sequences, i.e. $(\varepsilon, \varepsilon^2, \ldots)$ and $(\varepsilon^\lambda, \varepsilon^{2\lambda}, \ldots)$. From equation (45) the accuracy of the composite solutions is up to $O(\varepsilon^2)$ or $O(\varepsilon^{2\lambda})$, depending on whether $\lambda > 1$ or $\lambda < 1$. The value of λ as evaluated with equation (21) is $\lambda = -\gamma_m F(0) = -\gamma_m \exp[-\gamma_m T_a^*/(\gamma_T + \gamma_m T_\infty^*)]$.

5. RESULTS AND DISCUSSIONS

There are six parameters, i.e., Pe, Le, γ_m, γ_T, T_a^* and T_∞^*, in the problem under consideration. It is difficult to cover all the interested cases by changing these parameters. Because $\varepsilon = Pe^{-1/2}$ is chosen as the small parameter for perturbation analysis, $Pe = 100$ is fixed in all numerical computations while varying other parameters. The values of $(Le, \gamma_m, \gamma_T, T_a^*) = (1, -20, 15, 20, 8)$ are used as reference; when one parameter is varied the other four parameters are fixed.

To demonstrate the accuracy of approximation at different orders, the profiles of concentration and temperature for parameters at the reference values are shown in Fig. 3 where the dashed curves are the $O(1)$ results and the solid curves include the $O(\varepsilon^\lambda)$ corrections. Apparently, higher order correction is more profound for the concentration than for the temperature, especially near the impermeable heated wall. The inclusion of the $O(\varepsilon^\lambda)$ terms is needed to satisfy the zero mass flux condition of the concentration at the wall. Figure 3 shows that the concentration continuously decreases as the fluid moves toward the wall. The depletion of the reactant is about 96%. The temperature profile shown in Fig. 3 indicates that the porous medium is cooled first since the reaction is endothermic when $\gamma_T = 15$. The medium near the impermeable wall is then heated up by the wall. The minimum temperature occurs at $y/H \approx 0.25$ where the heat required for reaction is balanced by the heat through conduction.

The concentration and temperature profiles for different Le are depicted in Fig. 4. It is clear that the effect due to mass diffusivity on the concentration profiles is insignificant. This is because the diffusion process is confined in the thin thermal boundary layer. Most of the reaction takes place in the outer layer where the diffusion plays little role. Figure 4 also shows that the mass diffusion has almost no effect on the temperature profiles. Near the impermeable wall, the heat flux due to conduction is considerably larger than that taken by chemical reaction. This weak dependence on Le is also shown in Fig. 6 of Chao *et al.* [11] for the case of thick thermal boundary layer with exothermic reaction.

Figure 5 shows the concentration and temperature profiles for different values of reaction rate constant. Apparently, the concentration as well as the temperature are sensitive to the reaction rate. Higher reaction rate constant leads to more depletion of the reactant, so as to faster cooling of the incoming fluid. Again, the effect of varying γ_m is similar to that shown in Fig. 5a of Chao *et al.* [11] for the case of exothermic reaction.

In Fig. 6, we show the temperature and concentration profiles for different values of chemical reaction heat. We see that the chemical reaction heat has a very strong effect on the temperature, but only moderate on the concentration. This phenomena is anticipated, because the change in temperature caused by reaction leads only to small modifications of Arrhenius kinetics. Faster depletion for exothermic reaction than for endothermic reaction since the excess heat released by exothermic reaction is to heat up the reactant to promote the chemical reaction.

Figure 7 shows the effect of reaction activation energy on the concentration and temperature profiles. It is found that for endothermic reaction of $\gamma_T = 15$, large activation energy can greatly reduce the reaction rate. The lower activation level results in lower temperature in catalytic beds.

The effects of temperature of incoming fluid on the performance of the catalytic bed are shown in Fig. 8. These effects are mainly due to the change in the Arrhenius kinetics since the temperature difference ΔT is used for normalization. The figure shows that the initial fluid temperature plays a strong role in controlling the chemical reaction. Higher initial temperature results in faster reaction. The results shown in Fig. 8 are similar to those shown in Fig. 7. The increase in T_a^* has the effect equivalent to the decrease in T_∞^* because the Arrhenius kinetics is basically characterized by the ratio T_a^*/T_∞^*.

6. CONCLUDING REMARKS

In this paper, chemically reacting stagnation flows in catalytic beds has been studied. Singular per-

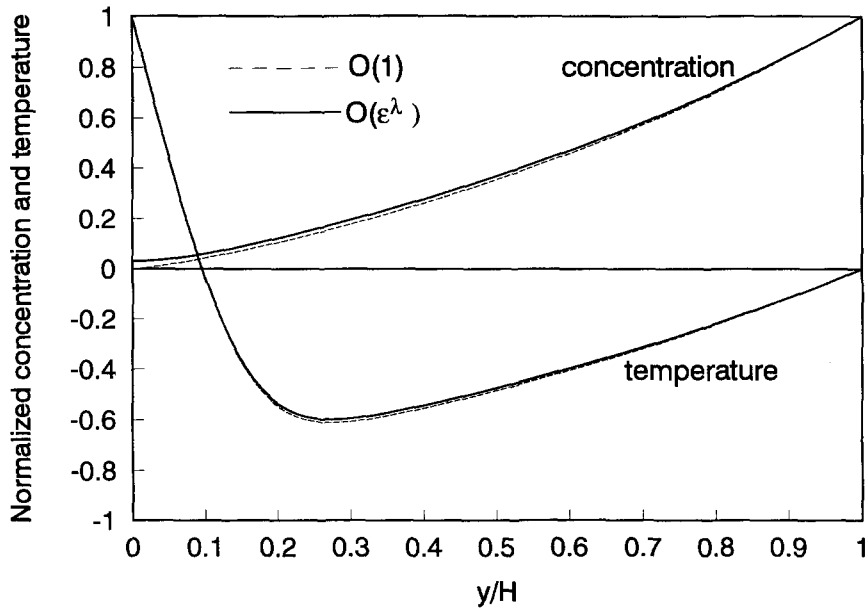

Fig. 3. The accuracy of the perturbation analysis at different orders. ($Pe = 100$. $Le = 1, \gamma_m = -20, \gamma_T = 15$, $T_a^* = 20, T_\infty^* = 8$.)

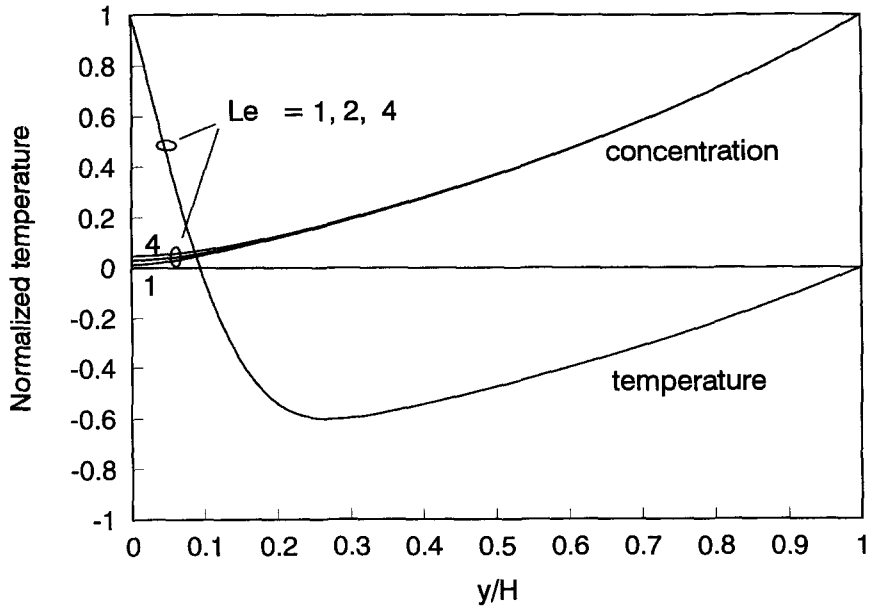

Fig. 4. The effect of Lewis number on concentration and temperature. ($Pe = 100, \gamma_m = -20, \gamma_T = 15$, $T_a^* = 20, T_\infty^* = 8$.)

turbation analysis was performed under the condition that the catalytic bed is much thicker than the thermal boundary layer. At a constant thickness ratio the results show that the reactant concentration is strongly dependent on the parameters related to the Arrhenius kinetics, but only weakly on whether the chemical reaction is endothermic or exothermic. The reason for such weak dependence on chemical reaction heat is because the change in fluid temperature does not lead to any significant change in the Arrhenius kinetics. Lower concentration is resulted from higher chemical reaction rate constant, lower activation energy or higher incoming fluid temperature. The effect due to mass diffusivity on concentration profiles is weak and confined in the diffusion layer near the impermeable wall. On this ground we can

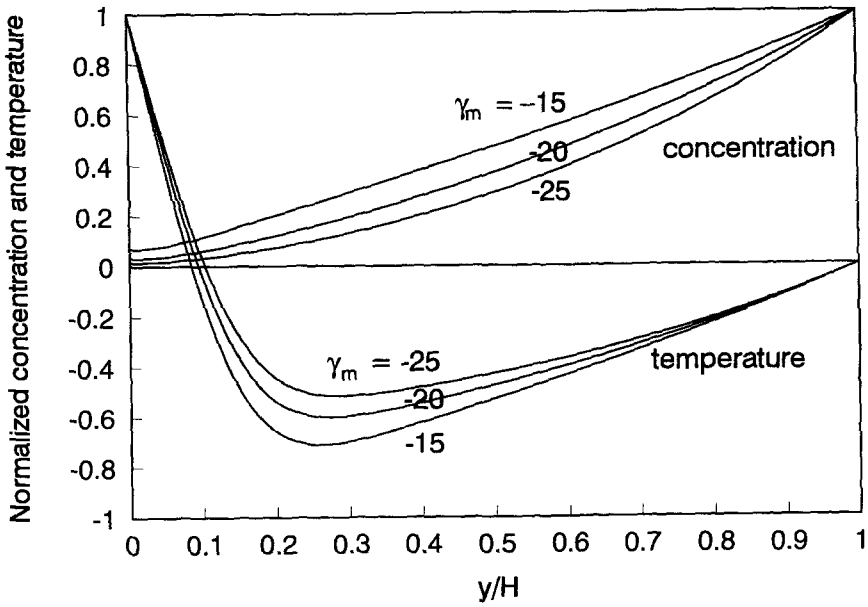

Fig. 5. The effect of chemical reaction rate constant on concentration and temperature. ($Pe = 100, Le = 1, \gamma_T = 15, T_a^* = 20, T_\infty^* = 8.$)

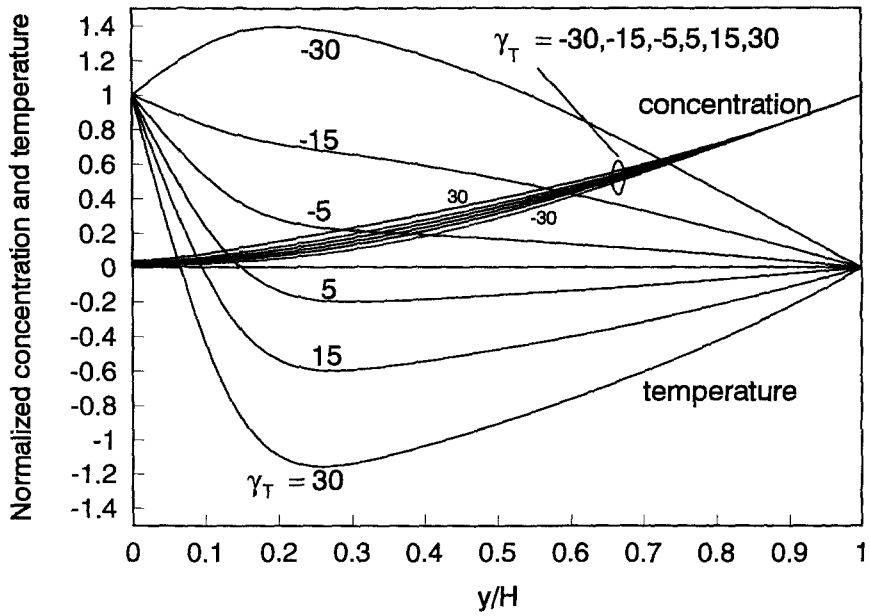

Fig. 6 The effect of chemical reaction heat on concentration and temperature. ($Pe = 100, Le = 1, \gamma_m = -20, T_\infty^* = 8.$)

infer that the effect due to the thermal conductivity on the reactant concentration is also weak and confined in the thermal boundary layer.

The present results show that the temperature in the catalytic bed depends strongly on chemical reaction heat and thermal conductivity, but only weakly on other parameters. The control of the wall temperature is essential in preventing the catalytic beds from being over-heated in strong exothermic reaction or under-cooled in strong endothermic reaction.

The present analysis includes the effects due to Brinkman's viscous layer The Brinkman's viscous effect changes greatly only the velocity component along the wall, but not the component normal to the wall. For stagnation flows the heat convection near the impermeable wall is mainly carried out by the

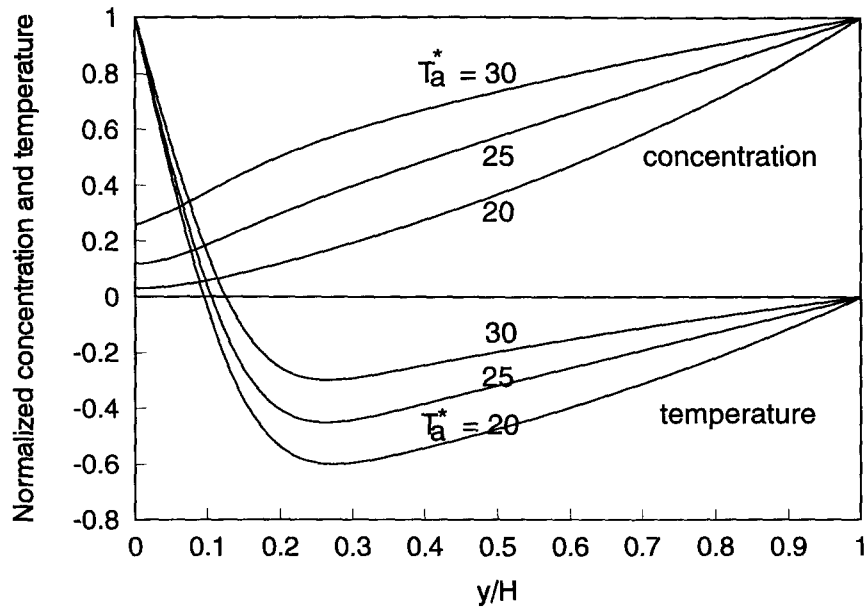

Fig. 7. The effect of activation energy on concentration and temperature. ($Pe = 100, Le = 1, \gamma_m = -20, \gamma_T = 15, T_\infty^* = 8.$)

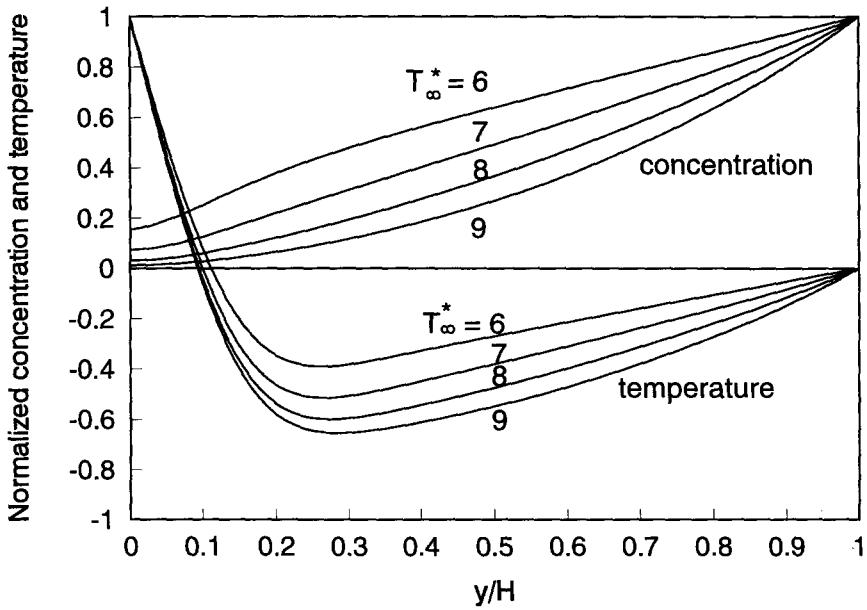

Fig. 8. The effect of incoming fluid temperature on concentration and temperature. ($Pe = 100, Le = 1, \gamma_m = -20, \gamma_T = 15, T_a^* = 20.$)

velocity component normal to the wall; therefore, the Brinkman's viscous effect is negligible in this study.

Acknowledgements—This work was supported by Chiang's Foundation through Grant No. RH92104 and by the Hong Kong Government through RGC Grant Nos. HKUST575/94E and HKUST815/96E. The comments of Profs P. Cheng and B. H. Chao during the course of this study are greatly appreciated.

REFERENCES

1. Elnashaie, S. S. E. H. and Elshishini, S. S., *Modeling, Simulation and Optimization of Industrial Fixed Bed Catalytic Reactors*. Gordon and Breach Science Publishers, 1993, p. 481.
2. Sathe, S. B., Kulkarni, M. R., Peck, R. E. and Tong, T. W., Experimental and theoretical study of porous radiant burner performance. *23rd Symp. (Int.) on Combustion*, 1991, pp. 1011–1018.

3. McDermott, J., Catalytic conversion of automobile exhaust. *Pollution Control Review*. Noyes Data Corporation, Park Ridge, NJ, 1971, **2.**
4. Chao, B. H. and Law, C. K., Asymptotic theory of flame extinction with surface reaction. *Comb. Flame*, 1993, **92,** 1–24.
5. Sato, J. and Tsuji, H., Extinction of premixed flames in a stagnation flow considering general Lewis number. *Combust. Sci. Tech*, 1983, **33,** 193–205.
6. Law, C. K. and Sivashinsky, G. I., Catalytic extension of extinction limits of stretched premixed flames. *Combust. Sci. Tech*, 1982, **29,** 277–286.
7. Giovangigli, V. and Candel, S., Extinction limits of premixed catalyzed flames in stagnation point flows. *Combust. Sci. Tech*, 1986, **48,** 1–30.
8. Viljoen, H. and Hlavacek, H., Chemically driven convection in a porous medium. *AIChE Journal*, 1987, **33,** 1344–1350.
9. Chen, Y. K., Hsu, P. F., Lim, I. G., Lu, Z. H., Matthews, R. D., Howell, J. D. and Nichols, S. P., Experimental and theoretical investigation of combustion within porous inert media. *22nd Symposium on Combustion*, 1988, pp. 202–207.
10. Chao, B. H., Cheng, P. and Le, T., Free-convective diffusion flame sheet in porous media, *Combust. Sci. Tech*, 1994, **99,** 221–234.
11. Chao, B. H., Wang, H. and Cheng, P., Stagnation point flow of a chemically reactive fluid in a catalytic porous bed. *International Journal of Heat and Mass Transfer*, 1996, **39,** 3003–3019.
12. Schlichting, H., *Boundary-Layer Theory*, 7th edn. McGraw-Hill, 1979.
13. Van Dyke, M., *Perturbation Methods in Fluid Mechanics*. Academic Press, New York, 1964.